arXiv:2504.13012v1 [cond-mat.mes-hall] 17 Apr 2025

# Hopf Exceptional Points

Tsuneya Yoshida,[1,2] Emil J. Bergholtz,[3] and Tomáš Bzdušek[4]

[1] *Department of Physics, Kyoto University, Kyoto 606-8502, Japan*
[2] *Institute for Theoretical Physics, ETH Zurich, 8093 Zurich, Switzerland*
[3] *Department of Physics, Stockholm University, AlbaNova University Center, 10691 Stockholm, Sweden*
[4] *Department of Physics, University of Zürich, Winterthurerstrasse 190, 8057 Zürich, Switzerland*

(Dated: April 18, 2025)

Exceptional points at which eigenvalues and eigenvectors of non-Hermitian matrices coalesce are ubiquitous in the description of a wide range of platforms from photonic or mechanical metamaterials to open quantum systems. Here, we introduce a class of *Hopf exceptional points* (HEPs) that are protected by the Hopf invariants (including the higher-dimensional generalizations) and which exhibit phenomenology sharply distinct from conventional exceptional points. Saliently, owing to their $\mathbb{Z}_2$ topological invariant related to the Witten anomaly, three-fold HEPs and symmetry-protected five-fold HEPs act as their own "antiparticles". Furthermore, based on higher homotopy groups of spheres, we predict the existence of multifold HEPs and symmetry-protected HEPs with non-Hermitian topology captured by a range of finite groups (such as $\mathbb{Z}_3$, $\mathbb{Z}_{12}$, or $\mathbb{Z}_{24}$) beyond the periodic table of Bernard-LeClair symmetry classes.

*Introduction.*—The notion of topology plays a pivotal role in modern condensed matter physics of both quantum [1–5] and classical systems [6–10]. Saliently, topological physics implies the possibility of various exotic quasiparticles. One of the prime examples is a Majorana zero mode [11–14] whose antiparticle is itself. In addition, a Weyl fermion [15–21], protected by Chern number in topological semimetals, is a source of negative magnetoresistance [22] which is a signal of chiral anomaly. The periodic table for the ten Altland-Zirnbauer symmetry classes provides a systematic understanding of the topological obstructions inducing these exotic excitations in Hermitian systems [23–29].

Notably, open systems coupled to environments host topological excitations for which non-Hermiticity is essential, such as exceptional points [30–35]. At exceptional points, two energy bands touch in both the real and the imaginary parts. Such band touchings are protected by the winding topology of energy eigenvalues [36]. In sharp contrast to Hermitian topological excitations, exceptional points exhibit a dispersion with a fractional exponent. Exceptional points and their variants [37–48] are reported for a wide range of platforms from quantum systems [49–58] to metamaterials [59–72], indicating the ubiquity of these non-Hermitian excitations. In particular, the high controllability of synthetic systems allows for the realization of exceptional points in dimensions $d$ larger than three [59, 60, 73–75].

Among the various exceptional points, multifold exceptional points exhibit an $n$-fold band touching [74–82]. These unique excitations are beyond the existing classification table for Bernard-LeClair symmetry classes [83–87] and discussed in interdisciplinary fields [64, 73, 88–101]. However, topology of the formerly reported $n$-fold exceptional points (EP$n$'s) is generally characterized by $\mathbb{Z}$ invariants [75, 76]. This, in particular, implies that an exceptional point cannot be its own "antiparticle".

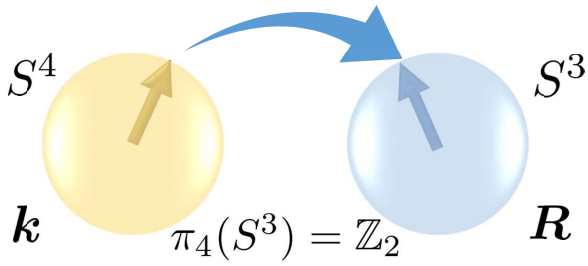


FIG. 1. Illustration of $\mathbb{Z}_2$ topology protecting an HEP3. The resultant vector $\boldsymbol{R}(\boldsymbol{k})$ defines a map from a 4-sphere in the momentum (or parameter) space to a 3-sphere in the space of the resultant vector [see Eqs. (1) and (2)]. If the map is topologically nontrivial, an HEP3 with $\mathbb{Z}_2$ topology exists inside the 4-sphere.

In this work, we report novel non-Hermitian topological excitations, dubbed $n$-fold Hopf exceptional points (HEP$n$'s, $n=3,4,5$). Saliently, an HEP3 and a symmetry-protected HEP5 exhibit unusual $\mathbb{Z}_2$ topology, meaning that they act as their own antiparticle. We trace this striking feature to the homotopy group $\pi_4(S^3)=\mathbb{Z}_2$ (see Fig. 1). We further discover symmetry-protected HEP4 whose topology is classified by $\pi_3(S^2)=\mathbb{Z}$. Leveraging higher homotopy groups of spheres, we elucidate the potential presence of HEP$n$'s characterized by abundant finite groups (e.g., $\mathbb{Z}_3$, $\mathbb{Z}_{12}$, and $\mathbb{Z}_{24}$) beyond the existing classification table.

*HEP3s with $\mathbb{Z}_2$ topology.*—As a first example, we consider a generic three-band non-Hermitian Hamiltonian $H(\boldsymbol{k})$ in a five-dimensional momentum (or parameter) space denoted by $\boldsymbol{k}=(k_1,\dots,k_5)$. Such a momentum space whose dimensionality is higher than three can be accessed in metamaterials [59, 60, 73–75]. The formation of an EP3 is captured by vanishing resultants $r_j\in\mathbb{C}$

$$r_j(\boldsymbol{k}) = \mathrm{Res}[\partial_E^{n-1-j}P(E,\boldsymbol{k}),\partial_E^{n-1}P(E,\boldsymbol{k})], \qquad (1)$$

with $j=1,2,\ldots,n-1$ and $n=3$ (see Supplemental Material [102] for basic information on resultants). Here, $P(E,\boldsymbol{k})=\det[H(\boldsymbol{k})-E\mathbb{1}]\in\mathbb{C}$ is the characteristic polynomial, and $\partial_E$ denotes derivative with respect to the polynomial variable $E\in\mathbb{C}$.

To expose whether the EP3 is in fact an HEP3, we consider a 4-sphere $S^4\subset\mathbb{R}^5$ enclosing the band touching. Assuming $(r_1,r_2)\neq(0,0)$ on the 4-sphere, we introduce a normalized vector $\boldsymbol{n}=\boldsymbol{R}/\|\boldsymbol{R}\|$ ($\|\boldsymbol{R}\|=\sqrt{\boldsymbol{R}\cdot\boldsymbol{R}}$) with the resultant vector

$$\boldsymbol{R}(\boldsymbol{k})=(\mathrm{Re}[r_1],\mathrm{Im}[r_1],\mathrm{Re}[r_2],\mathrm{Im}[r_2]). \tag{2}$$

Vector $\boldsymbol{n}(\boldsymbol{k})$ defines a map from $S^4$ to $S^3$ whose topology is classified by an element of the homotopy group $\pi_4(S^3)=\mathbb{Z}_2$. When the map of $\boldsymbol{n}(\boldsymbol{k})$ possesses nontrivial $\mathbb{Z}_2$ topology, the enclosed band touching is an HEP3.

The $\mathbb{Z}_2$ invariant $\nu_{\mathrm{F}}$ of maps from $S^4$ to $S^3$, originally discovered by Freudenthal [103], was considered in Ref. 104 in the context of the Witten anomaly in SU(2) gauge theory. Numerical computation of this $\mathbb{Z}_2$ invariant is carried out by the following representation [105]

$$\nu_{\mathrm{F}}=\frac{1}{4\pi}\oint d^4p\epsilon^{\mu\nu\rho\lambda}[\partial_\mu\Delta\varphi(\boldsymbol{p})]A_\nu F_{\rho\lambda} \tag{3}$$

with $\mu,\nu,\rho,\lambda=1,\ldots,4$ and anti-symmetric tensor $\epsilon^{\mu\nu\rho\lambda}$ taking $\epsilon^{1234}=1$. The Berry connection $A_\mu$ and the Berry curvature $F_{\mu\nu}$ are obtained from the *resultant Hamiltonian*, and the phase $\Delta\varphi(\boldsymbol{p})$ ($0\leq\Delta\varphi\leq 2\pi$) is obtained from the resultant vector. For the precise definitions of $A_\mu$, $F_{\mu\nu}$ and $\Delta\varphi$, see App. A. Vector $\boldsymbol{p}$ parametrizes the 4-sphere in the momentum space. While the integral in Eq. (3) can take an arbitrary integer value, gauge transformations can change $\nu_{\mathrm{F}}$ by multiples of two [104].

We demonstrate the emergence of an HEP3 in five dimensions by analyzing a toy model whose Hamiltonian reads

$$H=\begin{pmatrix}0&1&0\\0&0&1\\\frac{\zeta_2}{6}&\zeta_1&0\end{pmatrix}, \tag{4}$$

where the functions $\zeta_{1,2}(\boldsymbol{k})$ are parameterized by $\delta$, $m_0$, and $f(k_5)$ (for the explicit form, see App. B). Here the function $f(k_5)$ is either even [$f(k_5)=1$] or odd [$f(k_5)=2\sin(k_5/2)$].

The vanishing resultant vector $\boldsymbol{R}\propto(\mathrm{Re}\zeta_1,\mathrm{Im}\zeta_1,\mathrm{Re}\zeta_2,\mathrm{Im}\zeta_2)^{\mathrm{T}}=\boldsymbol{0}$ specifies where the HEP3s emerge in the momentum space. The explicit form of the resultant vector [see App. B] indicates the emergence of HEP3s at $\boldsymbol{k}=(0,0,0,\pi/2,\pm\pi/3)$ for $\delta=0.5$ and $m_0=1.5$. Figure 2(a,b) displays the emergence of the HEP3 at $\boldsymbol{k}=(0,0,0,\pi/2,\pi/3)$.

Notably, the HEP acts as its own antiparticle as a direct consequence of its $\mathbb{Z}_2$ topology. This fact is elucidated by examining pair annihilation of HEP3s in two cases: $f(k_5)=1$ and $f(k_5)=2\sin(k_5/2)$ [see Fig. 2(c,d)].

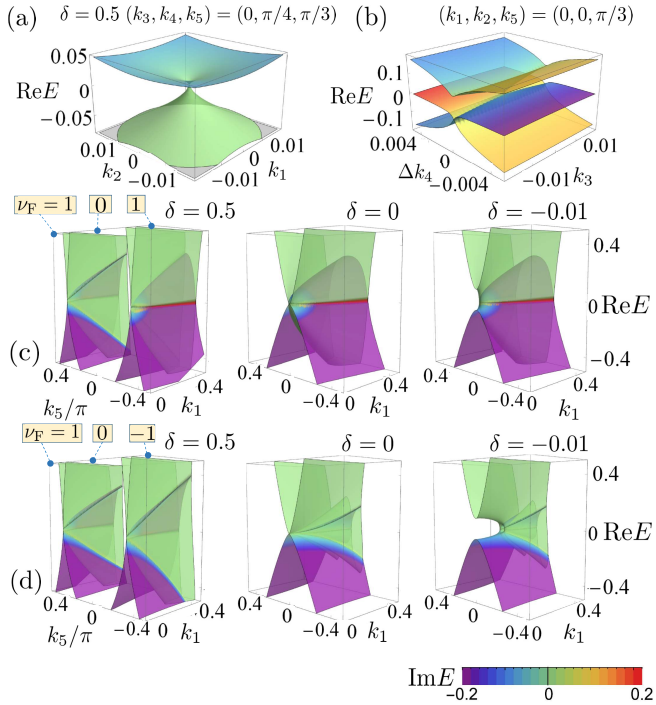


FIG. 2. Energy bands of Hamiltonian (4) for $m_0=1.5$. The real (imaginary) part is represented as height (color). In panel (a), the complex conjugate of the upper band is omitted. Panels (a) and (b) are obtained for $k_5=\pi/3$, $\delta=0.5$, and $f(k_5)=1$. Here, $\Delta k_4$ is defined as $\Delta k_4=k_4-\pi/2$. Panel (c) [(d)] displays pair annihilation of HEP3s for $(k_2,k_3,k_4)=(0,0,\pi/2)$, and $f(k_5)=1$ [$f(k_5)=2\sin(k_5/2)$]. In these panels, numerically computed $\nu_{\mathrm{F}}$ for $k_5=-\pi/2$, 0, and $\pi/2$ at $\delta=0.5$ is represented by numbers enclosed by blue squares. We used a mesh of $40^4$ points to evaluate the integrals. Momenta $k_{1,2,3}$ run from $-\pi$ to $\pi$, and $k_4$ runs from 0 to $2\pi$.

For $f(k_5)=1$ and $\delta=0.5$, the system hosts two HEP3s demarcated by the planes at $k_5=\pi/2$, 0 and $-\pi/2$ where numerically computed $\nu_{\mathrm{F}}$ is equal to 1, 0, and 1, respectively [for computation of $\nu_{\mathrm{F}}$, see App. C]. As $\delta$ decreases, the two HEP3s approach and annihilate each other [see Fig. 2(c)]. Changing the parity of $f(k_5)$ flips the sign of the numerically computed $\nu_{\mathrm{F}}$ at $k_5=-\pi/2$. Even in this case, pair annihilation occurs [see Fig. 2(d)]. The occurrence of pair annihilation in both arrangements manifests that HEP3s are indeed protected by $\mathbb{Z}_2$ topology, implying that an HEP3 is its own antiparticle.

*Symmetry-protected HEP5s with $\mathbb{Z}_2$ topology.*— Symmetry further enriches Hopf exceptional points, as exemplified by the emergence of symmetry-protected HEP5 in five dimensions. We consider a five-band non-Hermitian Hamiltonian which preserves parity-time ($PT$-) symmetry

$$U_{\mathrm{PT}}H^*(\boldsymbol{k})U_{\mathrm{PT}}^{-1}=H(\boldsymbol{k}) \tag{5}$$

with a unitary matrix satisfying $U_{\mathrm{PT}}U_{\mathrm{PT}}^*=\mathbb{1}$. Here, $\mathbb{1}$ is the identity matrix, and asterisks denote complex conju-

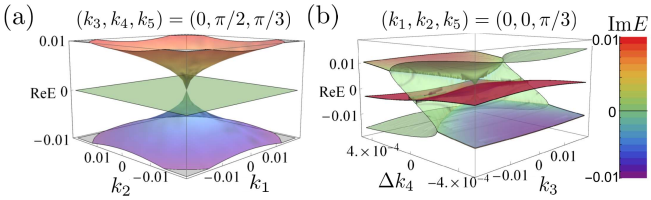


FIG. 3. Energy bands of Hamiltonian (8) for $f(k_5)=1$, $k_5=\pi/3$, $m_0=1.5$ and $\delta=0.5$. The real (imaginary) part is represented as height (color). Panel (a) [(b)] displays the data for $(k_3,k_4)=(0,\pi/2)$ [$(k_1,k_2)=(0,0)$]. In panel (a), the complex conjugates of the upper and the lower bands are omitted. In panel (b), $\Delta k_4$ is defined as $\Delta k_4 = k_4 - \pi/2$.

gation. The $PT$-symmetry imposes the constraint

$$P(E) = P^*(E^*), \tag{6}$$

indicating that all coefficients of the polynomial $P(E)$ are real. For $n=5$, the formation of an EP5 is captured by vanishing resultants $r_{1,\dots,4}=0$ [see Eq. (1)]. Due to $PT$-symmetry [see Eqs. (5) and (6)] these resultants are real: $r_{1,\dots,4} \in \mathbb{R}$. A similar argument applies to three other cases of symmetry [75, 76]: pseudo-Hermiticity, charge-conjugation-parity ($CP$-), and chiral symmetry [see App. D].

To expose whether the EP5 is in fact an HEP5, we consider a 4-sphere $S^4 \subset \mathbb{R}$ enclosing the band touching. Assuming $r_{1,\dots,4} \neq 0$ on the 4-sphere, we introduce a normalzied vector $\boldsymbol{n} = \boldsymbol{R}/\|\boldsymbol{R}\|$ with

$$\boldsymbol{R} = (r_1, r_2, r_3, r_4)^{\mathrm{T}}. \tag{7}$$

The normalized vector $\boldsymbol{n}$ defines a map from $S^4$ to $S^3$ whose topology is classified by $\pi_4(S^3)=\mathbb{Z}_2$. When the map of $\boldsymbol{n}$ possesses nontrivial $\mathbb{Z}_2$ topology, the enclosed band touching is a symmetry-protected HEP5. The topological invariant is introduced in a similar way as Eq. (3) with the only difference that we compute the $\mathbb{Z}_2$ invariant from the resultant vector in Eq. (7) instead of the one in Eq. (2).

We demonstrate the emergence of a symmetry-protected HEP5 by analyzing a toy model whose Hamiltonian reads

$$H = \begin{pmatrix} 0 & 1 & 0 & 0 & 0 \\ 0 & 0 & 1 & 0 & 0 \\ 0 & 0 & 0 & 1 & 0 \\ 0 & 0 & 0 & 0 & 1 \\ \frac{\zeta_4}{(5!)^3} & \frac{\zeta_3}{(5!)^2} & \frac{\zeta_2}{5!2!} & \frac{\zeta_1}{3!} & 0 \end{pmatrix} \tag{8}$$

with real functions $\zeta_{1\dots,4}(\boldsymbol{k})$ parameterized by $\delta$, $m_0$, and $f(k_5)$ [for the explicit form, see App. E]. Here, $f(k_5)$ is either $f(k_5)=1$ or $f(k_5)=2\sin(k_5/2)$. This Hamiltonian preserves $PT$-symmetry [Eq. (5)] with $U_{\mathrm{PT}}=\mathbb{1}$.

The vanishing resultant vector $\boldsymbol{R} \propto (\zeta_1,\zeta_2,\zeta_3,\zeta_4)^{\mathrm{T}} = \boldsymbol{0}$ specifies where the symmetry-protected HEP5s emerge.

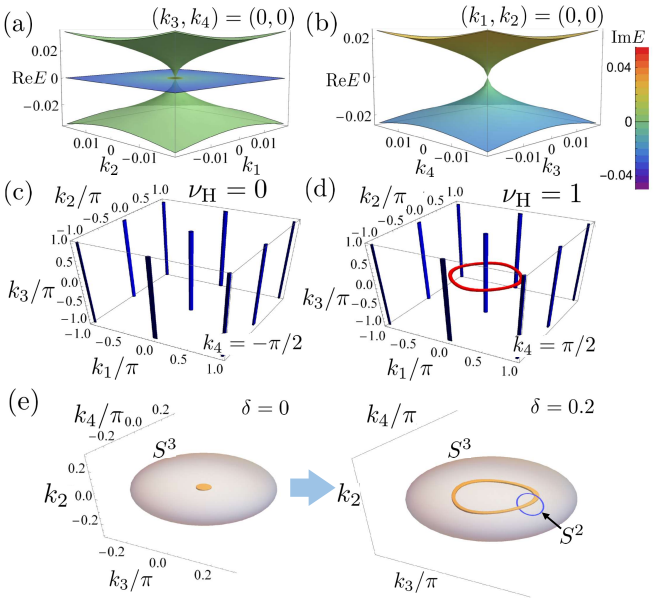


FIG. 4. (a) and (b): Energy eigenvalues of Hamiltonian (10) for $m_0=3$ and $\delta=0$. The real (imaginary) part is represented as height (color). In panel (b), complex conjugates of the upper and lower bands are omitted. (c) [(d)]: Lines in the momentum space $(k_1,k_2,k_3)$ for $m_0=3$, $\delta=0$ and $k_4=-\pi/2$ [$k_4=\pi/2$], where red and blue lines denote the momenta satisfying $\boldsymbol{R} \propto (0,0,1)^{\mathrm{T}}$ and $\boldsymbol{R} \propto (0,0,-1)^{\mathrm{T}}$, respectively. The linking of these lines determines the value of the Hopf invariant $\nu_{\mathrm{H}}$. (e): Momenta satisfying $\boldsymbol{R}(\boldsymbol{k})=\boldsymbol{0}$ for $k_1=0$ and $\delta=0$ resp. $\delta=0.2$ (orange manifolds). As $\delta$ is introduced, the symmetry-protected HEP4 inflates into a loop. The gray oval and the blue loop illustrate the $S^3$ resp. $S^2$, both extending in the fourth dimension $k_1$ (not shown), on which one computes the Hopf invariant $\nu_{\mathrm{H}}$ resp. the resultant winding number $W_2$ (see App. H) [75].

The explicit form of the resultant vector [see App. E] indicates that the model in Eq. (8) hosts symmetry-protected $\mathbb{Z}_2$ HEP5s at $\boldsymbol{k}=(0,0,0,\pi/2,\pm\pi/3)$ which possesses $\mathbb{Z}_2$ topological charge [see Fig. 3].

*Symmetry-protected HEP4s with $\mathbb{Z}$ topology.*— Symmetry protection also enables HEP4s with $\mathbb{Z}$ topology. To illustrate such a possibility, we consider a four-band non-Hermitian Hamiltonian with $PT$-symmetry [see Eq. (5)] in a four-dimensional momentum space described by $\boldsymbol{k}=(k_1,k_2,k_3,k_4)$. For $n=4$, the formation of an EP4 is captured by vanishing resultants $r_{1,\dots,3}=0$ [see Eq. (1)].

To expose whether the EP4 is in fact an HEP4, we consider a 3-sphere $S^3 \subset \mathbb{R}^4$ enclosing the band touching. The homotopy group $\pi_3(S^2)=\mathbb{Z}$ implies the existence of nontrivial maps $\boldsymbol{n}(\boldsymbol{k})=\boldsymbol{R}/\|\boldsymbol{R}\|$. When the map of $\boldsymbol{n}$ possesses nontrivial $\mathbb{Z}$ topology, the enclosed band touching is a symmetry-protected HEP4.

The topology of such HEP4s is characterized by the

Hopf invariant, expressed as [106–108]

$$\nu_{\rm H} = \oint \frac{d^3\boldsymbol{p}}{2} \epsilon^{\mu\nu\rho} A_\mu F_{\nu\rho}, \tag{9}$$

with $\mu, \nu, \rho = 1, 2, 3$. Here, $A_\mu$ and $F_{\mu\nu}$ are obtained from the resultant Hamiltonian (for the definitions, see App. A). Vector $\boldsymbol{p}$ parametrizes the 3-sphere in the momentum space.

We demonstrate the emergence of a symmetry-protected HEP4 by analyzing a toy model whose Hamiltonian reads

$$H = \begin{pmatrix} 0 & 1 & 0 & 0 \\ 0 & 0 & 1 & 0 \\ 0 & 0 & 0 & 1 \\ \frac{\zeta_3}{24^2} & -\frac{\zeta_2}{24} & \frac{\zeta_1}{2} & 0 \end{pmatrix}, \tag{10}$$

with real functions $\zeta_{1,\ldots,3}(\boldsymbol{k})$ parametrized by $\delta$ and $m_0$ [for the explicit form, see App. F].

The vanishing resultant vector $\boldsymbol{R} \propto (\zeta_1, \zeta_2, \zeta_3)^{\rm T} = \boldsymbol{0}$ specifies where the symmetry-protected HEP4 emerges in the momentum space. The explicit form of the resultant [see App. F] indicates the emergence of a symmetry-protected HEP4 at $\boldsymbol{k} = \boldsymbol{0}$ for $m_0 = 3$ [see Fig. 4(a,b)]. Here, we characterize the symmetry-protected HEP4 enclosed by two planes at $k_4 = -\pi/2$ and $k_4 = \pi/2$. Numerically evaluating the Hopf invariant [Eq. (9)], we obtain $\nu_{\rm H} = 0$ [$\nu_{\rm H} = 1$] for $k_4 = -\pi/2$ [$k_4 = \pi/2$] which is consistent with linking of the inverse maps in the momentum space [see Fig. 4(c,d)] [109, 110]. These results indicate that the symmetry-protected HEP4 is characterized by $\nu_{\rm H} = 1$.

*Multiply-charged aspect of HEPs.*—Reference 76 has pointed out that the codimension of symmetry-protected EP4s is three, whereas the codimension of the HEP4 in our model is four [see Fig. 4(a,b)]. This mismatch in codimension implies that the HEP4 may inflate into a loop of EP4s [see Fig. 4(e)]. Such a perturbation does not trivialize the Hopf topology but enriches it [29]: the loop of EP4s carries both the Hopf invariant on $S^3$ and the resultant winding number on $S^2$. In the same spirit, a similar assignment of multiple topological invariants applies to all HEPs introduced in this work.

*Additional bands.*—So far, we have discussed HEP$n$'s in $n$-band models. For systems with more than $n$ bands, EP$n$'s are still associated with winding of the resultant vector; however, the converse does not hold. Specifically, as discussed in App. G, it is possible to find situations where a finite value of the winding number leads to the vanishing resultant vector $\boldsymbol{R} = \boldsymbol{0}$ without a symmetry-protected EP3.

Nevertheless, topological invariants of resultants are applicable when we focus around an HEP$n$ (or an EP$n$). Specifically, if we know that an HEP$n$ emerges at momenta $\boldsymbol{k} = \boldsymbol{k}_0$ and energy $E = E_0$, we may apply the Taylor expansion to the characteristic polynomial $P(E) = \det[H(\boldsymbol{k}) - E\mathbb{1}]$, which leads to a polynomial $\tilde{P}(\tilde{E})$ with degree $n$

$$\tilde{P}(\tilde{E}) = \sum_{j=0}^{n} a_j(\boldsymbol{k}) \tilde{E}^j, \tag{11}$$

with $a_j(\boldsymbol{k})$ $(j = 0, 1, \ldots, n)$ being complex functions and $\tilde{E} = E - E_0$. Computing the topological invariant [e.g., Eq. (3)] of $\tilde{P}(\tilde{E})$ around $\boldsymbol{k} = \boldsymbol{k}_0$, we can characterize the HEP$n$ for systems with more than $n$ bands.

| $c$ | HEP3<br>SP-HEP4, SP-HEP5 | SP-HEP6 | HEP4<br>SP-HEP7 |
|---|---|---|---|
| 3 | $\mathbb{Z}$ | 0 | 0 |
| 4 | $\mathbb{Z}_2$ | $\mathbb{Z}$ | 0 |
| 5 | $\mathbb{Z}_2$ | $\mathbb{Z}_2$ | $\mathbb{Z}$ |
| 6 | $\mathbb{Z}_{12}$ | $\mathbb{Z}_2$ | $\mathbb{Z}_2$ |
| 7 | $\mathbb{Z}_2$ | $\mathbb{Z} \times \mathbb{Z}_{12}$ | $\mathbb{Z}_2$ |
| 8 | $\mathbb{Z}_2$ | $\mathbb{Z}_2^2$ | $\mathbb{Z}_{24}$ |
| 9 | $\mathbb{Z}_3$ | $\mathbb{Z}_2^2$ | $\mathbb{Z}_2$ |
| 10 | $\mathbb{Z}_{15}$ | $\mathbb{Z}_{24} \times \mathbb{Z}_3$ | $\mathbb{Z}_2$ |
| 11 | $\mathbb{Z}_2$ | $\mathbb{Z}_{15}$ | $\mathbb{Z}_2$ |
| 12 | $\mathbb{Z}_2^2$ | $\mathbb{Z}_2$ | $\mathbb{Z}_{30}$ |
| 13 | $\mathbb{Z}_{12} \times \mathbb{Z}_2$ | $\mathbb{Z}_2^3$ | $\mathbb{Z}_2$ |
| 14 | $\mathbb{Z}_{84} \times \mathbb{Z}_2^2$ | $\mathbb{Z}_{120} \times \mathbb{Z}_{12} \times \mathbb{Z}_2$ | $\mathbb{Z}_2^3$ |
| 15 | $\mathbb{Z}_2^2$ | $\mathbb{Z}_{84} \times \mathbb{Z}_2^5$ | $\mathbb{Z}_{72} \times \mathbb{Z}_2$ |

TABLE I. HEPs are classified by homotopy groups of spheres. The topology explicitly analyzed in this manuscript corresponds to the blue entries. HEP$n$'s [symmetry-protected HEP$n$'s] of codimension $c = 3, 4, \ldots$ are classified by $\pi_c(S^{2n-3})$ [$\pi_c(S^{n-2})$].

*Higher dimensions.*—Higher homotopy groups of spheres indicate abundant topology of HEP$n$'s. HEP$n$'s are captured by the $(2n-2)$-component resultant vector, and thus are classified by $\pi_c(S^{2n-3})$ with codimension $c \geq 3$. Symmetry-protected HEP$n$'s are captured by the $(n-1)$-component resultant vector, and thus are classified by $\pi_c(S^{n-2})$. The classification results for HEP$n$'s $(n = 3, 4)$ and symmetry-protected HEP$n$'s $(n = 4, 5, 6, 7)$ are summarized in Table I (see also Sec. 4.1 of Ref. [111] and Chapter XIV of Ref. [112]). This table predicts the presence of various HEP$n$'s following exotic fusion rules. For instance, $\mathbb{Z}_3$ topology of codimension $c = 9$ implies an HEP3 annihilate with two copies of itself, which is reminiscent of parafermions [113–116]. In addition, there exist HEP3s with $\mathbb{Z}_{12}$ topology of codimension $c = 6$ and HEP4s with $\mathbb{Z}_{24}$ topology of codimension $c = 8$.

*Discussion.*—We have discovered novel non-Hermitian topological excitations, dubbed Hopf exceptional points. Saliently, HEP3s and symmetry-protected HEP5s exhibit an unusual $\mathbb{Z}_2$ topology, meaning that they act as their own antiparticle. This striking feature arises from the homotopy group $\pi_4(S^3) = \mathbb{Z}_2$. We have further discovered symmetry-protected HEP4s whose topology is

classified by $\pi_3(S^2)=\mathbb{Z}$. Leveraging higher homotopy groups of spheres, we elucidate the potential presence of HEP$n$'s characterized by abundant finite groups (e.g., $\mathbb{Z}_3$, $\mathbb{Z}_{12}$, and $\mathbb{Z}_{24}$) beyond the classification table of Bernard-LeClair symmetry classes.

Our work on non-Hermitian multiband systems opens up a new direction of topological physics. Here, we outline several concrete open questions motivated by our findings. (*i*) The high controllability of metamaterials allows access to momentum (or parameter) spaces with dimensions larger than three [59, 60, 73–75], thus inviting realistic experimental verifications of the unusual topology of HEP$n$'s. (*ii*) Table I implies the presence of novel HEPs following a unique fusion rule due to their topology. Explicit analysis based on topological invariants and concrete models is an interesting issue. (*iii*) Unless the band structure is provided, one-to-one correspondence between EP$n$'s and the resultant winding numbers is lost for many-band systems. This observation calls for more general characterization of EP$n$ topology. (*iv*) Finally, it is interesting to consider non-Hermitian topological bands, captured by suitably adapted Hopf invariants [110], that arise in models with a hopfion texture [117] of the resultant vector over the Brillouin zone torus.

*Acknowledgments.*—T. Y. is supported by JSPS KAKENHI Grant Nos. JP21K13850, and JP23KK0247, JSPS Bilateral Program No. JPJSBP120249925. T. Y. is grateful for the support from the ETH Pauli Center for Theoretical Studies and the Grant from Yamada Science Foundation. E. J. B. is supported by the Wallenberg Scholars program (2023.0256) and the Göran Gustafsson Foundation for Research in Natural Sciences and Medicine. T. B. was supported by the Starting Grant No. 211310 by the Swiss National Science Foundation (SNSF).

[1] M. Z. Hasan and C. L. Kane, Colloquium: Topological insulators, Rev. Mod. Phys. **82**, 3045 (2010).
[2] X.-L. Qi and S.-C. Zhang, Topological insulators and superconductors, Rev. Mod. Phys. **83**, 1057 (2011).
[3] C. L. Kane and E. J. Mele, $Z_2$ Topological Order and the Quantum Spin Hall Effect, Phys. Rev. Lett. **95**, 146802 (2005).
[4] C. L. Kane and E. J. Mele, Quantum Spin Hall Effect in Graphene, Phys. Rev. Lett. **95**, 226801 (2005).
[5] X.-L. Qi, T. L. Hughes, and S.-C. Zhang, Topological field theory of time-reversal invariant insulators, Phys. Rev. B **78**, 195424 (2008).
[6] F. D. M. Haldane and S. Raghu, Possible Realization of Directional Optical Waveguides in Photonic Crystals with Broken Time-Reversal Symmetry, Phys. Rev. Lett. **100**, 013904 (2008).
[7] L. Lu, J. D. Joannopoulos, and M. Soljačić, Topological photonics, Nat. Photonics **8**, 821 (2014).
[8] E. Prodan and C. Prodan, Topological Phonon Modes and Their Role in Dynamic Instability of Microtubules, Phys. Rev. Lett. **103**, 248101 (2009).
[9] V. V. Albert, L. I. Glazman, and L. Jiang, Topological Properties of Linear Circuit Lattices, Phys. Rev. Lett. **114**, 173902 (2015).
[10] C. H. Lee, S. Imhof, C. Berger, F. Bayer, J. Brehm, L. W. Molenkamp, T. Kiessling, and R. Thomale, Topolectrical circuits, Commun. Phys. **1**, 39 (2018).
[11] A. Y. Kitaev, Unpaired Majorana fermions in quantum wires, Phys.-Uspekhi **44**, 131 (2001).
[12] G. Moore and N. Read, Nonabelions in the fractional quantum hall effect, Nucl. Phys. B **360**, 362 (1991).
[13] N. Read and D. Green, Paired states of fermions in two dimensions with breaking of parity and time-reversal symmetries and the fractional quantum Hall effect, Phys. Rev. B **61**, 10267 (2000).
[14] L. Fu and C. L. Kane, Superconducting Proximity Effect and Majorana Fermions at the Surface of a Topological Insulator, Phys. Rev. Lett. **100**, 096407 (2008).
[15] H. Weyl, Elektron und Gravitation. I, Z. Phys. **56**, 330 (1929).
[16] S. Murakami, Phase transition between the quantum spin Hall and insulator phases in 3D: emergence of a topological gapless phase, New J. Phys. **9**, 356 (2007).
[17] X. Wan, A. M. Turner, A. Vishwanath, and S. Y. Savrasov, Topological semimetal and Fermi-arc surface states in the electronic structure of pyrochlore iridates, Phys. Rev. B **83**, 205101 (2011).
[18] A. A. Burkov and L. Balents, Weyl Semimetal in a Topological Insulator Multilayer, Phys. Rev. Lett. **107**, 127205 (2011).
[19] B. Yan and C. Felser, Topological Materials: Weyl Semimetals, Annu. Rev. Condens. Matter Phys. **8**, 337 (2017).
[20] S.-Y. Xu, I. Belopolski, N. Alidoust, M. Neupane, G. Bian, C. Zhang, R. Sankar, G. Chang, Z. Yuan, C.-C. Lee, S.-M. Huang, H. Zheng, J. Ma, D. S. Sanchez, B. Wang, A. Bansil, F. Chou, P. P. Shibayev, H. Lin, S. Jia, and M. Z. Hasan, Discovery of a Weyl fermion semimetal and topological Fermi arcs, Science **349**, 613 (2015).
[21] B. Q. Lv, H. M. Weng, B. B. Fu, X. P. Wang, H. Miao, J. Ma, P. Richard, X. C. Huang, L. X. Zhao, G. F. Chen, Z. Fang, X. Dai, T. Qian, and H. Ding, Experimental Discovery of Weyl Semimetal TaAs, Phys. Rev. X **5**, 031013 (2015).
[22] X. Huang, L. Zhao, Y. Long, P. Wang, D. Chen, Z. Yang, H. Liang, M. Xue, H. Weng, Z. Fang, X. Dai, and G. Chen, Observation of the Chiral-Anomaly-Induced Negative Magnetoresistance in 3D Weyl Semimetal TaAs, Phys. Rev. X **5**, 031023 (2015).
[23] A. P. Schnyder, S. Ryu, A. Furusaki, and A. W. W. Ludwig, Classification of topological insulators and superconductors in three spatial dimensions, Phys. Rev. B **78**, 195125 (2008).
[24] A. Kitaev, Periodic table for topological insulators and superconductors, AIP Conf. Proc. **1134**, 22 (2009).
[25] Shinsei Ryu and Andreas P Schnyder and Akira Furusaki and Andreas W W Ludwig, Topological insulators and superconductors: tenfold way and dimensional hierarchy, New J. Phys. **12**, 065010 (2010).
[26] K. Shiozaki and M. Sato, Topology of crystalline insulators and superconductors, Phys. Rev. B **90**, 165114 (2014).
[27] T. Morimoto and A. Furusaki, Weyl and Dirac semimetals with $\mathbb{Z}_2$ topological charge, Phys. Rev. B **89**, 235127

(2014).
[28] C.-K. Chiu and A. P. Schnyder, Classification of reflection-symmetry-protected topological semimetals and nodal superconductors, Phys. Rev. B **90**, 205136 (2014).
[29] T. Bzdušek and M. Sigrist, Robust doubly charged nodal lines and nodal surfaces in centrosymmetric systems, Phys. Rev. B **96**, 155105 (2017).
[30] I. Rotter, A non-Hermitian Hamilton operator and the physics of open quantum systems, J. Phys. A **42**, 153001 (2009).
[31] T. Katō, *Perturbation theory for linear operators* (Springer, New York, 1966).
[32] W. D. Heiss, The physics of exceptional points, J. Phys. A **45**, 444016 (2012).
[33] M. V. Berry, Physics of Nonhermitian Degeneracies, Czech. J. Phys. **54**, 1039 (2004).
[34] E. J. Bergholtz, J. C. Budich, and F. K. Kunst, Exceptional topology of non-Hermitian systems, Rev. Mod. Phys. **93**, 015005 (2021).
[35] Y. Ashida, Z. Gong, and M. Ueda, Non-Hermitian physics, Adv. Phys. **69**, 249 (2020).
[36] H. Shen, B. Zhen, and L. Fu, Topological Band Theory for Non-Hermitian Hamiltonians, Phys. Rev. Lett. **120**, 146402 (2018).
[37] Y. Xu, S.-T. Wang, and L.-M. Duan, Weyl Exceptional Rings in a Three-Dimensional Dissipative Cold Atomic Gas, Phys. Rev. Lett. **118**, 045701 (2017).
[38] J. Carlström and E. J. Bergholtz, Exceptional links and twisted Fermi ribbons in non-Hermitian systems, Phys. Rev. A **98**, 042114 (2018).
[39] X.-Q. Sun, C. C. Wojcik, S. Fan, and T. Bzdušek, Alice strings in non-Hermitian systems, Phys. Rev. Res. **2**, 023226 (2020).
[40] C. C. Wojcik, X.-Q. Sun, T. Bzdušek, and S. Fan, Homotopy characterization of non-Hermitian Hamiltonians, Phys. Rev. B **101**, 205417 (2020).
[41] J. C. Budich, J. Carlström, F. K. Kunst, and E. J. Bergholtz, Symmetry-protected nodal phases in non-Hermitian systems, Phys. Rev. B **99**, 041406 (2019).
[42] R. Okugawa and T. Yokoyama, Topological exceptional surfaces in non-Hermitian systems with parity-time and parity-particle-hole symmetries, Phys. Rev. B **99**, 041202 (2019).
[43] H. Zhou, J. Y. Lee, S. Liu, and B. Zhen, Exceptional surfaces in PT-symmetric non-Hermitian photonic systems, Optica **6**, 190 (2019).
[44] T. Yoshida, R. Peters, N. Kawakami, and Y. Hatsugai, Symmetry-protected exceptional rings in two-dimensional correlated systems with chiral symmetry, Phys. Rev. B **99**, 121101 (2019).
[45] K. Kimura, T. Yoshida, and N. Kawakami, Chiral-symmetry protected exceptional torus in correlated nodal-line semimetals, Phys. Rev. B **100**, 115124 (2019).
[46] Z. Yang, A. P. Schnyder, J. Hu, and C.-K. Chiu, Fermion Doubling Theorems in Two-Dimensional Non-Hermitian Systems for Fermi Points and Exceptional Points, Phys. Rev. Lett. **126**, 086401 (2021).
[47] M. M. Denner, A. Skurativska, F. Schindler, M. H. Fischer, R. Thomale, T. Bzdušek, and T. Neupert, Exceptional topological insulators, Nat. Commun. **12**, 5681 (2021).
[48] T. Yoshida, R. Okugawa, and Y. Hatsugai, Discriminant indicators with generalized inversion symmetry, Phys. Rev. B **105**, 085109 (2022).
[49] V. Kozii and L. Fu, Non-Hermitian topological theory of finite-lifetime quasiparticles: Prediction of bulk Fermi arc due to exceptional point, Phys. Rev. B **109**, 235139 (2024).
[50] A. A. Zyuzin and A. Y. Zyuzin, Flat band in disorder-driven non-Hermitian Weyl semimetals, Phys. Rev. B **97**, 041203 (2018).
[51] T. Yoshida, R. Peters, and N. Kawakami, Non-Hermitian perspective of the band structure in heavy-fermion systems, Phys. Rev. B **98**, 035141 (2018).
[52] T. Yoshida, R. Peters, N. Kawakami, and Y. Hatsugai, Exceptional band touching for strongly correlated systems in equilibrium, Prog. Theor. Exp. Phys. **2020**, 12A109 (2020).
[53] H. Shen and L. Fu, Quantum Oscillation from In-Gap States and a Non-Hermitian Landau Level Problem, Phys. Rev. Lett. **121**, 026403 (2018).
[54] Y. Nagai, Y. Qi, H. Isobe, V. Kozii, and L. Fu, DMFT Reveals the Non-Hermitian Topology and Fermi Arcs in Heavy-Fermion Systems, Phys. Rev. Lett. **125**, 227204 (2020).
[55] M. Am-Shallem, R. Kosloff, and N. Moiseyev, Exceptional points for parameter estimation in open quantum systems: analysis of the Bloch equations, New J. Phys. **17**, 113036 (2015).
[56] F. Minganti, A. Miranowicz, R. W. Chhajlany, and F. Nori, Quantum exceptional points of non-Hermitian Hamiltonians and Liouvillians: The effects of quantum jumps, Phys. Rev. A **100**, 062131 (2019).
[57] M. Nakagawa, N. Kawakami, and M. Ueda, Exact Liouvillian Spectrum of a One-Dimensional Dissipative Hubbard Model, Phys. Rev. Lett. **126**, 110404 (2021).
[58] W. Chen, M. Abbasi, B. Ha, S. Erdamar, Y. N. Joglekar, and K. W. Murch, Decoherence-Induced Exceptional Points in a Dissipative Superconducting Qubit, Phys. Rev. Lett. **128**, 110402 (2022).
[59] C. Dembowski, H.-D. Gräf, H. L. Harney, A. Heine, W. D. Heiss, H. Rehfeld, and A. Richter, Experimental Observation of the Topological Structure of Exceptional Points, Phys. Rev. Lett. **86**, 787 (2001).
[60] S.-B. Lee, J. Yang, S. Moon, S.-Y. Lee, J.-B. Shim, S. W. Kim, J.-H. Lee, and K. An, Observation of an Exceptional Point in a Chaotic Optical Microcavity, Phys. Rev. Lett. **103**, 134101 (2009).
[61] J. Doppler, A. A. Mailybaev, J. Böhm, U. Kuhl, A. Girschik, F. Libisch, T. J. Milburn, P. Rabl, N. Moiseyev, and S. Rotter, Dynamically encircling an exceptional point for asymmetric mode switching, Nature **537**, 76 (2016).
[62] B. Zhen, C. W. Hsu, Y. Igarashi, L. Lu, I. Kaminer, A. Pick, S.-L. Chua, J. D. Joannopoulos, and M. Soljačić, Spawning rings of exceptional points out of dirac cones, Nature **525**, 354 (2015).
[63] K. Takata and M. Notomi, Photonic Topological Insulating Phase Induced Solely by Gain and Loss, Phys. Rev. Lett. **121**, 213902 (2018).
[64] H. Zhou, C. Peng, Y. Yoon, C. W. Hsu, K. A. Nelson, L. Fu, J. D. Joannopoulos, M. Soljačić, and B. Zhen, Observation of bulk Fermi arc and polarization half charge from paired exceptional points, Science **359**, 1009 (2018).
[65] H. Meng, Y. S. Ang, and C. H. Lee, Exceptional points in non-Hermitian systems: Applications and recent de-

velopments, Appl. Phys. Lett. **124**, 060502 (2024).
[66] T. Ozawa, H. M. Price, A. Amo, N. Goldman, M. Hafezi, L. Lu, M. C. Rechtsman, D. Schuster, J. Simon, O. Zilberberg, and I. Carusotto, Topological photonics, Rev. Mod. Phys. **91**, 015006 (2019).
[67] M.-A. Miri and A. Alú, Exceptional points in optics and photonics, Science **363**, eaar7709 (2019).
[68] X. Zhu, H. Ramezani, C. Shi, J. Zhu, and X. Zhang, $\mathcal{PT}$-Symmetric Acoustics, Phys. Rev. X **4**, 031042 (2014).
[69] C. Shi, M. Dubois, Y. Chen, L. Cheng, H. Ramezani, Y. Wang, and X. Zhang, Accessing the exceptional points of parity-time symmetric acoustics, Nat. Commun. **7**, 11110 (2016).
[70] T. Yoshida and Y. Hatsugai, Exceptional rings protected by emergent symmetry for mechanical systems, Phys. Rev. B **100**, 054109 (2019).
[71] T. Hofmann, T. Helbig, F. Schindler, N. Salgo, M. Brzezińska, M. Greiter, T. Kiessling, D. Wolf, A. Vollhardt, A. Kabaši, C. H. Lee, A. Bilušić, R. Thomale, and T. Neupert, Reciprocal skin effect and its realization in a topolectrical circuit, Phys. Rev. Res. **2**, 023265 (2020).
[72] Y. Li, Y.-G. Peng, L. Han, M.-A. Miri, W. Li, M. Xiao, X.-F. Zhu, J. Zhao, A. Alù, S. Fan, and C.-W. Qiu, Anti-parity-time symmetry in diffusive systems, Science **364**, 170 (2019).
[73] W. Tang, X. Jiang, K. Ding, Y.-X. Xiao, Z.-Q. Zhang, C. T. Chan, and G. Ma, Exceptional nexus with a hybrid topological invariant, Science **370**, 1077 (2020).
[74] W. Tang, K. Ding, and G. Ma, Realization and topological properties of third-order exceptional lines embedded in exceptional surfaces, Nat. Commun. **14**, 6660 (2023).
[75] T. Yoshida, J. L. K. König, L. Rødland, E. J. Bergholtz, and M. Stålhammar, Winding topology of multifold exceptional points, Phys. Rev. Res. **7**, L012021 (2025).
[76] P. Delplace, T. Yoshida, and Y. Hatsugai, Symmetry-Protected Multifold Exceptional Points and their Topological Characterization, Phys. Rev. Lett. **127**, 186602 (2021).
[77] I. Mandal and E. J. Bergholtz, Symmetry and Higher-Order Exceptional Points, Phys. Rev. Lett. **127**, 186601 (2021).
[78] S. Sayyad and F. K. Kunst, Realizing exceptional points of any order in the presence of symmetry, Phys. Rev. Res. **4**, 023130 (2022).
[79] A. Montag and F. K. Kunst, Symmetry-induced higher-order exceptional points in two dimensions, Phys. Rev. Res. **6**, 023205 (2024).
[80] K. Yang and I. Mandal, Enhanced eigenvector sensitivity and algebraic classification of sublattice-symmetric exceptional points, Phys. Rev. B **107**, 144304 (2023).
[81] G. Demange and E.-M. Graefe, Signatures of three coalescing eigenfunctions, J. Phys. A **45**, 025303 (2011).
[82] M. Stålhammar and L. Rødland, Abelian Spectral Topology of Multifold Exceptional Points, arXiv:2412.15323 [cond-mat.mes-hall] (2024).
[83] K. Kawabata, T. Bessho, and M. Sato, Classification of Exceptional Points and Non-Hermitian Topological Semimetals, Phys. Rev. Lett. **123**, 066405 (2019).
[84] Z. Gong, Y. Ashida, K. Kawabata, K. Takasan, S. Higashikawa, and M. Ueda, Topological Phases of Non-Hermitian Systems, Phys. Rev. X **8**, 031079 (2018).
[85] K. Kawabata, S. Higashikawa, Z. Gong, Y. Ashida, and M. Ueda, Topological unification of time-reversal and particle-hole symmetries in non-Hermitian physics, Nat. Commun. **10**, 297 (2019).
[86] K. Kawabata, K. Shiozaki, M. Ueda, and M. Sato, Symmetry and Topology in Non-Hermitian Physics, Phys. Rev. X **9**, 041015 (2019).
[87] H. Zhou and J. Y. Lee, Periodic table for topological bands with non-Hermitian symmetries, Phys. Rev. B **99**, 235112 (2019).
[88] Z. Lin, A. Pick, M. Lončar, and A. W. Rodriguez, Enhanced Spontaneous Emission at Third-Order Dirac Exceptional Points in Inverse-Designed Photonic Crystals, Phys. Rev. Lett. **117**, 107402 (2016).
[89] J. Schnabel, H. Cartarius, J. Main, G. Wunner, and W. D. Heiss, $\mathcal{PT}$-symmetric waveguide system with evidence of a third-order exceptional point, Phys. Rev. A **95**, 053868 (2017).
[90] J. Wiersig, Revisiting the hierarchical construction of higher-order exceptional points, Phys. Rev. A **106**, 063526 (2022).
[91] K. Wang, L. Xiao, H. Lin, W. Yi, E. J. Bergholtz, and P. Xue, Experimental simulation of symmetry-protected higher-order exceptional points with single photons, Sci. Adv. **9**, eadi0732 (2023).
[92] H. Hodaei, A. U. Hassan, S. Wittek, H. Garcia-Gracia, R. El-Ganainy, D. N. Christodoulides, and M. Khajavikhan, Enhanced sensitivity at higher-order exceptional points, Nature **548**, 187 (2017).
[93] K. Bai, J.-Z. Li, T.-R. Liu, L. Fang, D. Wan, and M. Xiao, Nonlinear Exceptional Points with a Complete Basis in Dynamics, Phys. Rev. Lett. **130**, 266901 (2023).
[94] Q. Liu, D. A. Kessler, and E. Barkai, Designing exceptional-point-based graphs yielding topologically guaranteed quantum search, Phys. Rev. Res. **5**, 023141 (2023).
[95] Y. S. S. Patil, J. Höller, P. A. Henry, C. Guria, Y. Zhang, L. Jiang, N. Kralj, N. Read, and J. G. E. Harris, Measuring the knot of non-Hermitian degeneracies and non-commuting braids, Nature **607**, 271 (2022).
[96] A. Leclerc, L. Jezequel, N. Perez, A. Bhandare, G. Laibe, and P. Delplace, Exceptional ring of the buoyancy instability in stars, Phys. Rev. Res. **6**, L012055 (2024).
[97] L. Crippa, J. C. Budich, and G. Sangiovanni, Fourth-order exceptional points in correlated quantum many-body systems, Phys. Rev. B **104**, L121109 (2021).
[98] M. Stålhammar and E. J. Bergholtz, Classification of exceptional nodal topologies protected by $\mathcal{PT}$ symmetry, Phys. Rev. B **104**, L201104 (2021).
[99] N. Hatano, Exceptional points of the Lindblad operator of a two-level system, Mol. Phys. **117**, 2121 (2019).
[100] S. Khandelwal, N. Brunner, and G. Haack, Signatures of Liouvillian Exceptional Points in a Quantum Thermal Machine, PRX Quantum **2**, 040346 (2021).
[101] Y. Wu, Y. Wang, X. Ye, W. Liu, Z. Niu, C.-K. Duan, Y. Wang, X. Rong, and J. Du, Third-order exceptional line in a nitrogen-vacancy spin system, Nat. Nanotechnol. **19**, 160 (2024).
[102] Supplemental Material presents basic information about the resultant of two polynomials.
[103] H. Freudenthal, Topological properties of linear circuit lattices, Compos. Math. **5**, 299 (1938).
[104] E. Witten, Current algebra, baryons, and quark confinement, Nucl. Phys. B **223**, 433 (1983).
[105] T. Schuster, S. Gazit, J. E. Moore, and N. Y. Yao,

Floquet Hopf Insulators, Phys. Rev. Lett. **123**, 266803 (2019).
[106] J. E. Moore, Y. Ran, and X.-G. Wen, Topological Surface States in Three-Dimensional Magnetic Insulators, Phys. Rev. Lett. **101**, 186805 (2008).
[107] D.-L. Deng, S.-T. Wang, C. Shen, and L.-M. Duan, Hopf insulators and their topologically protected surface states, Phys. Rev. B **88**, 201105 (2013).
[108] Z. Yang and J. Hu, Non-Hermitian Hopf-link exceptional line semimetals, Phys. Rev. B **99**, 081102 (2019).
[109] F. Wilczek and A. Zee, Linking Numbers, Spin, and Statistics of Solitons, Phys. Rev. Lett. **51**, 2250 (1983).
[110] R. Kennedy, Topological Hopf-Chern insulators and the Hopf superconductor, Phys. Rev. B **94**, 035137 (2016).
[111] A. Hatcher, *Algebraic topology* (Cambridge University Press, Cambridge, 2002).
[112] H. Toda, *Composition methods in homotopy groups of spheres*, 49 (Princeton University Press, 1962).
[113] N. Read and E. Rezayi, Beyond paired quantum Hall states: Parafermions and incompressible states in the first excited Landau level, Phys. Rev. B **59**, 8084 (1999).
[114] P. Fendley, Parafermionic edge zero modes in Zn-invariant spin chains, J. Stat. Mech.: Theory Exp. **2012** (11), P11020.
[115] R. S. K. Mong, D. J. Clarke, J. Alicea, N. H. Lindner, P. Fendley, C. Nayak, Y. Oreg, A. Stern, E. Berg, K. Shtengel, and M. P. A. Fisher, Universal Topological Quantum Computation from a Superconductor-Abelian Quantum Hall Heterostructure, Phys. Rev. X **4**, 011036 (2014).
[116] H. Liu, R. Perea-Causin, and E. J. Bergholtz, Parafermions in moirè minibands, Nat. Commun. **16**, 1770 (2025).
[117] F. N. Rybakov, N. S. Kiselev, A. B. Borisov, L. Döing, C. Melcher, and S. Blügel, Magnetic hopfions in solids, APL Mater. **10**, 111113 (2022).

## End Matter

*Appendix A: Berry connection and curvature of the resultant Hamiltonian in Eqs. (3) and (9) .—* The $\mathbb{Z}_2$ invariant in Eq. (3) is obtained from the resultant vector $\boldsymbol{R}=(R_1,R_2,R_3,R_4)^{\mathrm{T}}$ ($R_{1,\ldots,4}\in\mathbb{R}$). Specifically, the Berry connection $A_\mu$ and the Berry curvature $F_{\mu\nu}$ are defined as

$$A_\mu = \frac{1}{2\pi \mathrm{i}}\langle z|\partial_\nu z\rangle, \tag{A12}$$

$$F_{\mu\nu} = \frac{1}{2\mathrm{i}}\Big(\langle\partial_\mu z|\partial_\nu z\rangle - \langle\partial_\nu z|\partial_\mu z\rangle\Big), \tag{A13}$$

with the negative eigenstate $|z\rangle$ of the resultant Hamiltonian $\tilde{\boldsymbol{n}}\cdot\boldsymbol{\sigma}$ with $\tilde{\boldsymbol{n}}=\tilde{\boldsymbol{R}}/\|\tilde{\boldsymbol{R}}\|$ and $\tilde{\boldsymbol{R}}=(R_1,R_2,R_3)$. Here, $\sigma_{1,\ldots,3}$ denote Pauli matrices. The ratio $\|\tilde{\boldsymbol{R}}\|/R_4$ defines the phase $\Delta\varphi(\boldsymbol{p})=2\varphi(\boldsymbol{p})$ with $\varphi=\arctan\|\tilde{\boldsymbol{R}}\|/R_4$ ($0\le\varphi\le\pi$). Substituting $\Delta\varphi$, $A_\mu$, and $F_{\mu\nu}$ into Eq. (3) yields the $\mathbb{Z}_2$ invariant $\nu_{\mathrm{F}}$.

The $\mathbb{Z}$ invariant in Eq. (9) is also obtained from the resultant vector $\boldsymbol{R}=(R_1,R_2,R_3)^{\mathrm{T}}$ ($R_{1,\ldots,3}\in\mathbb{R}$). Specifically, the Berry connection $A_\mu$ and the Berry curvature $F_{\mu\nu}$ are defined in the same way as Eqs. (A12) and (A13) except for the definition of $|z\rangle$. In this case, $|z\rangle$ is defined as the negative eigenstate of the resultant Hamiltonian $\boldsymbol{n}\cdot\boldsymbol{\sigma}$ with $\boldsymbol{n}=\boldsymbol{R}/\|\boldsymbol{R}\|$. Substituting the specific form of the Berry curvature $A_\mu$ and the Berry connection $F_{\mu\nu}$ into Eq. (9) yields $\mathbb{Z}$ invariant $\nu_{\mathrm{H}}$.

*Appendix B: Details of the model in Eq. (4).—* The explicit form of $\zeta$'s is

$$\zeta_1 = -2\sin\phi\Big(\eta_\uparrow^*\eta_\downarrow\Big), \tag{B14a}$$

$$\zeta_2 = -\sin\phi\Big(|\eta_\uparrow|^2-|\eta_\downarrow|^2\Big)+\mathrm{i}\cos\phi. \tag{B14b}$$

Here $\eta_\uparrow$, $\eta_\downarrow$ and $\phi$ are defined as

$$\eta_\uparrow = \sin k_1 + \mathrm{i}f(k_5)\sin k_2, \tag{B15a}$$

$$\eta_\downarrow = \sin k_3 + \mathrm{i}\Big[\xi(\boldsymbol{k})+\frac{3}{2}\sin k_4 - 3(\cos k_5+\delta)\Big], \tag{B15b}$$

$$\phi = \frac{\pi}{2}(1-\cos k_4), \tag{B15c}$$

with $\xi(\boldsymbol{k})=\sum_{j=1,2,3}\cos k_j - m_0$ and $f(k_5)$ being $f(k_5)=1$ or $f(k_5)=2\sin(k_5/2)$.

The resultant vector $\boldsymbol{R}$ is obtained as

$$\boldsymbol{R} = (3!)^2\Big(-2\sin\phi\mathrm{Re}[\eta_\uparrow\eta_\downarrow], -2\sin\phi\mathrm{Im}[\eta_\uparrow\eta_\downarrow], -\sin\phi(|\eta_\uparrow|^2-|\eta_\downarrow|^2), \cos\phi\Big)^{\mathrm{T}}. \tag{B16}$$

The above equation indicates that the resultant vector vanishes when $\eta_\uparrow=\eta_\downarrow=0$ and $\phi=\pi/2$ both hold.

*Appendix C: Computation of the $\mathbb{Z}_2$ invariant $\nu_{\mathrm{F}}$ for the toy model in Eq. (4) .—* From the given resultant vector [see Eq. (B16)], the $\mathbb{Z}_2$ invariant $\nu_{\mathrm{F}}$ is obtained as follows. With $\tilde{\boldsymbol{n}}=\tilde{\boldsymbol{R}}/\|\tilde{\boldsymbol{R}}\|$ and Eq. (B16), the resultant Hamiltonian is obtained as

$$\tilde{\boldsymbol{n}}\cdot\boldsymbol{\sigma} = -\frac{1}{\sqrt{|\eta_\uparrow|^2+|\eta_\downarrow|^2}}\begin{pmatrix}|\eta_\uparrow|^2-|\eta_\downarrow|^2 & 2\eta_\uparrow\eta_\downarrow^* \\ 2\eta_\uparrow^*\eta_\downarrow & -|\eta_\uparrow|^2+|\eta_\downarrow|^2\end{pmatrix}. \tag{C17}$$

Thus, the negative eigenstate of $\tilde{\boldsymbol{n}}\cdot\boldsymbol{\sigma}$ is obtained as

$$|z(\boldsymbol{k})\rangle = \frac{1}{\sqrt{|\eta_\uparrow|^2+|\eta_\downarrow|^2}}\begin{pmatrix}\eta_\uparrow \\ \eta_\downarrow\end{pmatrix}. \tag{C18}$$

In addition, from the resultant vector in Eq. (B16), we obtain

$$\Delta\varphi = 2\arctan\|\tilde{\boldsymbol{R}}\|/R_4 = 2\phi. \tag{C19}$$

Substituting the obtained $|z\rangle$ and $\Delta\varphi$ into Eq. (3), we can numerically compute the $\mathbb{Z}_2$ invariant.

*Appendix D: Three other cases of symmetry: pseudo-Hermicity, $CP$-, and chiral symmetry.—* The argument of $PT$-symmetry protected HEPs can be applied to other cases of symmetry: pseudo-Hermiticity, $CP$-, and chiral symmetry. We consider a Hamiltonian preserving pseudo-Hermiticity

$$U_{\mathrm{pH}}H(\boldsymbol{k})U_{\mathrm{pH}}^\dagger = H^\dagger(\boldsymbol{k}) \tag{D20}$$

with $U_{\mathrm{pH}}^\dagger$ being a unitary matrix and dagger denotes Hermitian conjugation. Because the transposition does not affect the determinant, Eq. (D20) leads to Eq. (6), implying that the resultants [Eq. (1)] are real.

For $CP$- and chiral symmetry, the Hamiltonian obeys

$$U_{\mathrm{CP}}H^*(\boldsymbol{k})U_{\mathrm{CP}}^\dagger = -H(\boldsymbol{k}), \tag{D21}$$

$$U_\Gamma H^\dagger(\boldsymbol{k})U_\Gamma^\dagger = -H(\boldsymbol{k}) \tag{D22}$$

with $U_{\mathrm{CP}}$ and $U_\Gamma$ being unitary matrices. In these cases, replacing $H$ to $H'=iH$ reduces to the case of $PT$-symmetry or pseudo-Hermiticity. Therefore, symmetry-protected HEP$n$'s may emerge when systems preserve pseudo-Hermiticity, $CP$-, or chiral symmetry.

*Appendix E: Details of the model in Eq. (8).—* The explicit form of $\zeta$'s are

$$\zeta_1+\mathrm{i}\zeta_2 = -2\sin\phi(\eta_\uparrow\eta_\downarrow), \tag{E23a}$$

$$\zeta_3 = -\sin\phi(|\eta_\uparrow|^2-|\eta_\downarrow|^2), \tag{E23b}$$

$$\zeta_4 = \cos\phi, \tag{E23c}$$

with $\eta$'s and $\phi$ defined in Eq. (B15).

The resultant vector of this Hamiltonian is obtained as

$$\boldsymbol{R} = (5!)^2\Big(-2\sin\phi\mathrm{Re}[\eta_\uparrow\eta_\downarrow], -2\sin\phi\mathrm{Im}[\eta_\uparrow\eta_\downarrow], -\sin\phi(|\eta_\uparrow|^2-|\eta_\downarrow|^2), \cos\phi\Big)^{\mathrm{T}}, \tag{E24}$$

which is proportional to the resultant vector in Eq. (B16). The above equation indicates that the resultant vector vanishes when $\eta_\uparrow = \eta_\downarrow = 0$ and $\phi = \pi/2$ both hold.

*Appendix F: Details of the model in Eq. (10).—* The explicit form of $\zeta$'s are

$$\zeta_1 + \mathrm{i}\zeta_2 = 2(\eta_\uparrow^* \eta_\downarrow), \tag{F25a}$$

$$\zeta_3 = |\eta_\uparrow|^2 - |\eta_\downarrow|^2 + \delta. \tag{F25b}$$

Here $\eta_\uparrow$ and $\eta_\downarrow$ are

$$\eta_\uparrow = \sin k_1 + \mathrm{i} \sin k_2, \tag{F26a}$$

$$\eta_\downarrow = \sin k_3 + \mathrm{i}\Big[\xi(\boldsymbol{k}) + \sin k_4\Big], \tag{F26b}$$

with $\xi(\boldsymbol{k}) = \sum_{j=1,2,3} \cos k_j - m_0$.

The resultant vector $\boldsymbol{R}$ is obtained as

$$\boldsymbol{R} = -(24)^2 \Big(2\mathrm{Re}[\eta_\uparrow^* \eta_\downarrow], 2\mathrm{Im}[\eta_\uparrow^* \eta_\downarrow], |\eta_\uparrow|^2 - |\eta_\downarrow|^2 + \delta\Big)^{\mathrm{T}}. \tag{F27}$$

The above equation indicates that the resultant vector vanishes when $\eta_\uparrow = 0$ and $|\eta_\downarrow| = \sqrt{\delta}$ both hold for $\delta > 0$ or when $\eta_\downarrow = 0$ and $|\eta_\uparrow| = \sqrt{|\delta|}$ both hold for $\delta < 0$.

*Appendix G: Fake EP3s.—* For three-band systems, EP3s with $PT$-symmetry are characterized by the resultant winding number [75, 76] of the resultant Hamiltonian $R_1\sigma_1 + R_2\sigma_2$ with $\boldsymbol{R} = (r_1, r_2)$ which satisfies chiral symmetry. However, for systems with four or more bands, the resultant winding number may additionally capture "fake EP3s" unless Taylor expansion is applied. This is because the resultant vector may vanish without a triple root in the characteristic polynomial $P(E)$ whose degree is four or higher.

As an example, we consider a non-Hermitian Hamiltonian

$$H = \begin{pmatrix} 1 + \mathrm{i}k_1 & 0 & 0 & 0 \\ 0 & 1 - \mathrm{i}k_1 & 0 & 0 \\ 0 & 0 & \mathrm{i}k_2 & 1 \\ 0 & 0 & 1 & -\mathrm{i}k_2 \end{pmatrix}, \tag{G28}$$

satisfying $PT$-symmetry [Eq. (5)] with

$$U_{\mathrm{PT}} = \begin{pmatrix} 0 & 1 & 0 & 0 \\ 1 & 0 & 0 & 0 \\ 0 & 0 & 1 & 0 \\ 0 & 0 & 0 & 1 \end{pmatrix}. \tag{G29}$$

The resultant winding number is defined as

$$W_1 = \oint \frac{dp}{2\pi \mathrm{i}} \partial_p \log[R_1(p) + \mathrm{i}R_2(p)], \tag{G30}$$

where $p$ parametrizes the circle in the momentum space. The winding number $W_1$ (see App. H) is finite for the path illustrated by the black arrow in Fig. G5(a). However, the system does not host EP3s [see Fig. G5(b)].

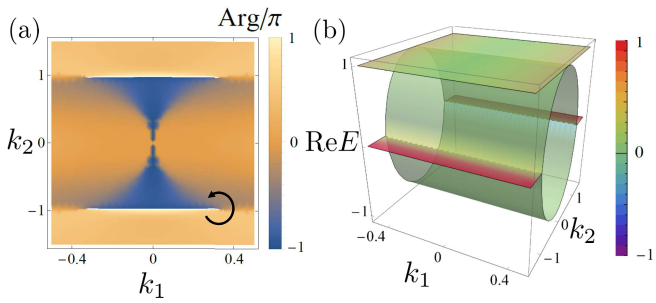


FIG. G5. (a) [(b)]: Argument of $R_1 + \mathrm{i}R_2$ [band structure] of Hamiltonian (G28). In panel (b), the complex conjugate of the top band is omitted.

*Appendix H: A brief review of resultant winding number.—* We consider an $N$-component resultant vector $\boldsymbol{R}(\boldsymbol{k})$ defined on an $N$-dimesional momentum space $\mathbb{R}^N$. When the norm is finite $\|\boldsymbol{R}\| \neq 0$ on an $(N-1)$-sphere $S^{N-1} \subset \mathbb{R}^N$, one can consider the normalized vector $\boldsymbol{n}(\boldsymbol{k}) = \boldsymbol{R}(\boldsymbol{k})/\|\boldsymbol{R}(\boldsymbol{k})\|$ whose topology is classified by $\pi_{N-1}(S^{N-1}) = \mathbb{Z}$.

The topology of such a map is characterized by the resultant winding number $W_{N-1}$ [75, 76]

$$W_{N-1} = \frac{\epsilon^{i_1 \cdots i_N}}{A_{N-1}} \int d^{N-1}\boldsymbol{p} f_{i_1 \cdots i_N}(\boldsymbol{p}), \tag{H31}$$

$$f_{i_1 \cdots i_N}(\boldsymbol{p}) = n_{i_1} \partial_1 n_{i_2} \partial_2 n_{i_3} \cdots \partial_{N-1} n_{i_N}, \tag{H32}$$

where the integral is taken over $S^{N-1}$ in the momentum space parameterized by vector $\boldsymbol{p}$. Here, the area of the $(N-1)$-dimensional sphere $A_{N-1}$ is expressed by

$$A_{2l-1} = \frac{2\pi^l}{(l-1)!}, \tag{H33}$$

$$A_{2l-2} = \frac{2^{2l-1}\pi^{l-1}(l-1)!}{(2l-2)!}, \tag{H34}$$

with a positive integer $l$.

The above invariant is rewritten as Chern numbers or winding numbers of the resultant Hamiltonian [76]. Specifically, for $N = 3$, Eq. (H31) is rewritten as the first Chern number of the resultant Hamiltonian $H_{\mathrm{R}}(\boldsymbol{k}) = \boldsymbol{R} \cdot \boldsymbol{\sigma}$. For $N = 4$, Eq. (H31) is rewritten as the winding number of three-dimensional chiral symmetric Hamiltonian $H_{\mathrm{R}} = \sum_{i=1,\ldots,4} R_i \gamma_i$ satisfying $\gamma_5 H_{\mathrm{R}} \gamma_5 = -H_{\mathrm{R}}$ with $\boldsymbol{\gamma} = (\sigma_1\tau_0, \sigma_2\tau_0, \sigma_3\tau_1, \sigma_3\tau_2, \sigma_3\tau_3)^{\mathrm{T}}$. Here, $\tau_{1,\ldots,3}$ are Pauli matrices, and $\tau_0$ is the $2 \times 2$ identity matrix. We note that the presence of the gap of $H_{\mathrm{R}}$ on the sphere is reduced to $\|\boldsymbol{R}\| \neq 0$. This is because the eigenvalues are given by $E_{\mathrm{R}} = \pm\|\boldsymbol{R}\|$ which arises from the anti-commutation relation $\{\gamma_i, \gamma_j\} = 2\delta_{ij}$.

# Supplemental Materials:
# **Hopf Exceptional Points**

### Appendix S1: A brief review of resultants

For given two polynomials

$$f(x) = a_n x^n + \ldots + a_1 x + a_0, \tag{S1}$$
$$g(x) = b_m x^m + \ldots + b_1 x + b_0, \tag{S2}$$

with complex coefficients $a$'s and $b$'s, the resultant is defined as

$$\mathrm{Res}[f(x), g(x)] = a_n^m b_m^n \prod_{i,j} (\alpha_i - \beta_j). \tag{S3}$$

Here, $\alpha$'s and $\beta$'s are roots of polynomials $f(x)$ and $g(x)$, respectively. Symbol $\prod_{i,j}$ denotes the product of all pairs of the roots. The resultant vanishes when the two polynomials have a common root.

The resultant can be computed from the Sylvester matrix

$$\mathrm{Res}[f(x), g(x)] = \det \begin{bmatrix} a_n & \cdots & a_0 & & & \\ & a_n & \cdots & a_0 & & \\ & & \ddots & & \ddots & \\ & & & a_n & \cdots & a_0 \\ b_m & \cdots & b_0 & & & \\ & b_m & \cdots & b_0 & & \\ & & \ddots & & \ddots & \\ & & & b_m & \cdots & b_0 \end{bmatrix}. \tag{S4}$$

Here, the empty elements are zero. The size of the matrix is $n+m$ and the first $n$ rows are composed of the coefficients $a$'s and the remaining $m$ rows are composed of the coefficients $b$'s.